Electrochemical Behaviors of Ferrocene Derivatives at an Electrode Modified with Terminally Substituted Alkanethiol Monolayer Assemblies

Kô Takehara* and Hiroyuki Takemura

Department of Chemistry, Faculty of Science, Kyushu University 01, Ropponmatsu, Fukuoka 810

(Received October 12, 1994)

Self-assembled monolayers of 11-mercapto-1-undecanol (MUO), 11-mercaptoundecanoic acid (MUA), and 11-amino-1-undecanethiol (AUT) were formed on a gold disk electrode. The effects of the terminal charges of these monolayers on the redox responses of 1,1′-ferrocenedimethanol (FcDM), (ferrocenylmethyl)trimethylammoniun bromide (FcMA) and ammonium ferrocenesulfonate (FcSA) were evaluated by using voltammetric (CV) techniques. The CV responses of FcDM and FcMA decreased in the order of MUA/Au (MUA modified gold electrode), MUO/Au, and AUT/Au. In contrast, the CV response of FcSA increased in the order of MUA/Au, MUO/Au, and AUT/Au. From these results, the effects of the terminal charges on the CV responses were measured in relation to the diffuse layer potential and the electrostatic interaction between the terminal unit and redox species.

A self-assembling method using the spontaneous adsorption of long-chain alkanethiols on a gold surface has been known to provide well-ordered, low defect, and electrically insulating monolayers.[1—8] The self-assembled monolayer has been expected to show various functionalities when the terminal CH_3 unit is replaced by other functional units.[9—17] One of the most attractive applications of the terminally substituted monolayer assembly is to fabricate a gold electrode surface with the monolayer. The voltammetric studies of the electroactive species anchored on the monolayer surface made clear the dependence of the electron-transfer rate on the distance between the electroactive species and the electrode metal surface, by changing the alkyl chain length of the monolayer.[18—21] On the other hand, Miller and Becka have reported the effect of the chain length of the ω-mercaptoalkanol monolayer on the redox response of the species in aqueous phase.[22—24] Analytical applications of the terminally substituted alkanethiol monolayers have also been reported by several authors.[25—31]

In our previous paper, we reported the effects of surface terminal units on the electrochemical responses of $[Fe(CN)_6]^{3-}$, $[Ru(NH_3)_6]^{3+}$, and 1,1′-ferrocenedimethanol (FcDM).[32] In the case of these redox species, however, the reduction processes of $[Fe(CN)_6]^{3-}$ and $[Ru(NH_3)_6]^{3+}$ and the oxidation process of FcDM should be compared to discuss the effect of the terminal unit. In this work, therefore, we prepared FcDM, (ferrocenylmethyl)trimethylammoniun bromide (FcMA) and ammonium ferrocenesulfonate (FcSA) for the redox species. We also prepared 11-mercapto-1-undecanol (MUO), 11-mercaptoundecanoic acid (MUA), and 11-amino-1-undecanethiol (AUT) for the terminally substituted monolayer constituent. Then, the effects of the terminal units of the monolayer formed on a gold electrode on the redox responses of these ferrocene derivatives were measured with voltammetric technique. The results are discussed in relation to the electrostatic interaction between the terminal units and redox species and to the effect of the terminal units on the diffuse layer potential.

Experimental

FcDM and FcMA were purchased from Tokyo Kasei Co. and Aldrich Chemical Company, respectively. FcSA was synthesized as follows: Solution of sulfuric acid (7.70 g, 78.5 mmol) in 30 dm^3 of dioxane was added by portions to a solution of ferrocene (15.0 g, 80.6 mmol) in 150 dm^3 of dioxane at room temperature and then the mixture was heated at 110 °C for 17 h. After cooling and evaporation, the residue was suspended in 100 dm^3 of water and insoluble materials were filtered off. Then the filtrate was made alkaline with aqueous ammonium and precipitated gold scales of FcSA were recrystallized from a mixture of ethanol–water. Yield, 3.99 g (52.5%). Anal. Calcd for $C_{10}H_{13}SO_3NFe{\cdot}H_2O$: C, 39.88; H, 5.02; N, 4.65%. Found: C, 39.91; H, 5.00; N, 4.63%. MUO and MUA were synthesized from 11-bromo-1-undecanol and 11-bromoundecanoic acid, respectively, by treatment with thiourea.[22] AUT was prepared in the way described previously.[32] The structures of the final products were confirmed by ^1H NMR (JEOL GSX-270, 270 MHz). All organic chemicals used for the synthesis were purchased from Tokyo Kasei Co. and used as supplied.

The modification of the self-assembled monolayer on a gold electrode was done in the following way. A gold disk electrode (Bioanalytical Systems Inc., 1.6 mm diameter)

was polished with alumina slurry on a felt pad (Buhler, Illinois), sonicated in distilled water, and air dried. Then the electrode was immersed in ethanolic solution containing 10 mM of thiol derivatives for 30 min. The modified electrode thus obtained was rinsed with ethanol, then distilled water (abbreviate as X-alk/Au). At this stage, all of the modified electrode surfaces were hydrophilic.

Cyclic voltammograms were recorded by using a Fuso Model 311 Polarograph, a Model 321B Potential-sweep unit, and Yokogawa Model 3655 digital recorder. An Ag/AgCl/3 M NaCl (aq) (1 M=1 mol dm^{-3}) and a platinum wire were used as the reference electrode and the counter electrode, respectively. All potential values are reported versus the Ag/AgCl reference electrode unless otherwise stated. The measurement were done in deoxygenated aqueous solution containing 2 mM ferrocene derivatives as the redox probe and 0.2 M KCl as the supporting electrolyte. The pH of the test solution was not adjusted to avoid unexpected effects of the buffer reagent. All the measurements were done at 25±0.5 °C. The oxidation process of the ferrocene derivatives (Fe(II) to Fe(III)) was analyzed for the discussion.

To confirm the reproducibility of the current–potential response, the preparation of the modified electrode and the voltammetric measurement were repeated at least two times for all of the experimental conditions examined. Although a slight distribution of a current-potential profile was observed at any modified electrode, the reproducibility was confirmed to be enough to differentiate the effects of terminal groups.

Results and Discussion

To obtain the formal redox potentials ($E^{0'}$) of FcDM, FcMA, and FcSA, the voltammograms were recorded with a bare Au electrode. All of the responses showed electrochemically reversible diffusion-controlled profiles, and therefore the mid-point potential of the anodic peak and cathodic peak was taken as the $E^{0'}$ value. The $E^{0'}$ values thus obtained were 0.284, 0.438, and 0.433 V for FcDM, FcMA, and FcSA, respectively. The diffusion coefficients of FcDM, FcMA, and FcSA were obtained from the dependence of the peak current on the square root of the potential scan rate to be 7.8×10^{-6}, 5.7×10^{-6}, and 5.4×10^{-6} cm^2 s^{-1}, respectively.

Figures 1, 2, and 3 show the stationary state voltammograms of 2 mM FcDM, FcMA, and FcSA, respectively, in 0.2 M KCl aqueous solution, which were observed at the bare Au and X-alk/Au electrodes. For all of the experimental conditions examined, the current–potential curves were scarcely affected by the repetition of the potential scan except in the reaction of FcMA at the AUT/Au electrode. In the reaction of FcMA at AUT/Au, the redox peak increased gradually with the cycles of the potential scan and the stationary state was attained only after several tens of cycles of the potential scan. As shown in Figs. 1 and 2, the electrochemical reversibility of the voltammetric response of FcDM and FcMA decreased in the order of MUA/Au>MUO/Au>AUT/Au. However, FcMA is more sensitive to change in the monolayer terminal unit than FcDM. Quite in contrast, the voltammetric

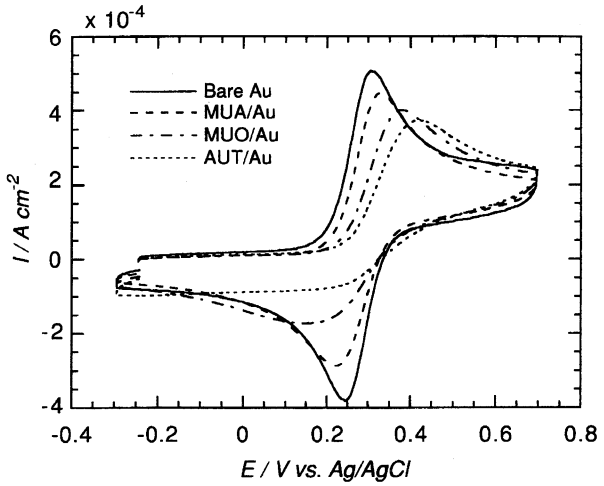

Fig. 1. Cyclic voltammograms of 2 mM FcDM in 0.2 M KCl aqueous solution obtained with bare Au and X-alk/Au electrodes at pH 5.80. Scan rate is 100 mV s^{-1}.

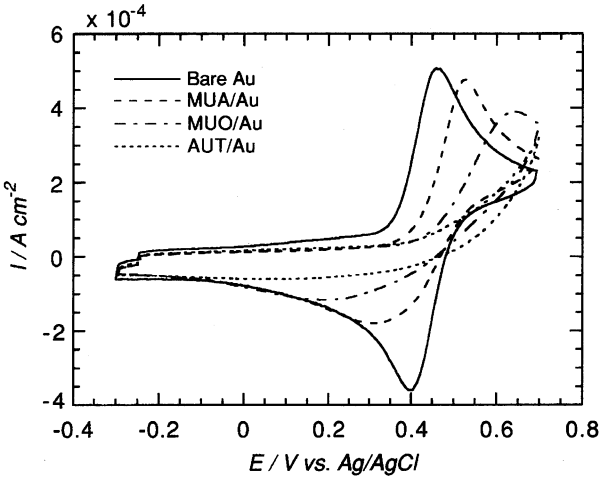

Fig. 2. Cyclic voltammograms of 2 mM FcMA in 0.2 M KCl aqueous solution obtained with bare Au and X-alk/Au electrodes at pH 5.62. Scan rate is 100 mV s^{-1}.

response of FcSA increased in the order of MUA/Au< MUO/Au<AUT/Au as shown in Fig. 3.

The acid dissociation constant (pK_a) of the MUA and AUT could not be obtained by potentiometric titration, because they are insoluble in aqueous solution. However, the pK_a values of 3-mercaptopropionic acid and 2-aminoethanethiol (they have the similar structures to MUA and AUT, respectively, with shorter hydrocarbon chains) have been reported to be 4.27[33] and 8.19,[34] respectively. By taking these pK_a values into account, the terminal COOH unit of MUA/Au and the NH_2 unit of AUT/Au are considered to be ionized to COO^- and NH_3^+, respectively, under the experimental conditions examined. It should be noted in this point that the ionization state of the surface confined units is different from the ionization state in the bulk of solution.[35] Condensed state of the terminal units in monolayer will hin-

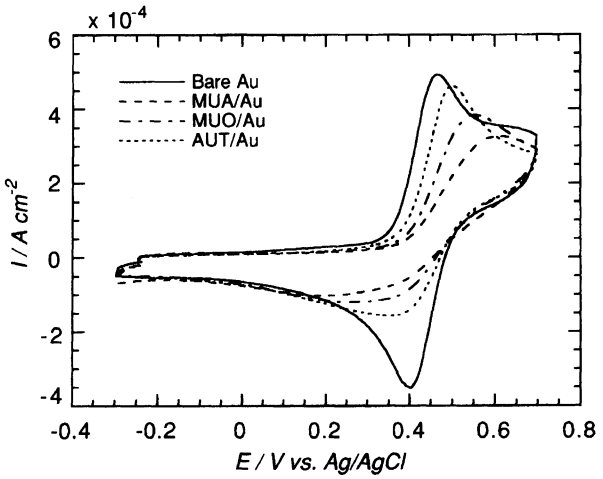

Fig. 3. Cyclic voltammograms of 2 mM FcSA in 0.2 M KCl aqueous solution obtained with bare Au and X-alk/Au electrodes at pH 5.73. Scan rate is 100 mV s^{-1}.

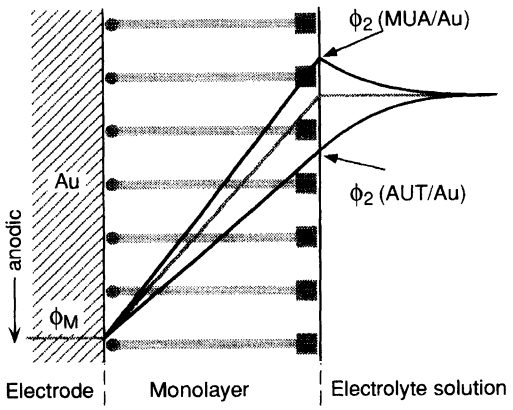

Fig. 4. Schematic illustration of the potential profiles at the monolayer modified electrode. The potential profiles at the MUA/Au and AUT/Au are presented based on the MUO/Au. The effective potential difference, $\Delta\phi_M - \Delta\phi_2$, driving the oxidation reaction is smaller at AUT/Au than at MUO/Au and the opposite effect is expected at MUA/Au.

der the full ionization of the terminal units due to electrostatic repulsion. Therefore, we cannot expect the full ionization state of the terminal units but only the partial ionization of the units, which is discussed in more detail later.

The following two different contributions of the ionized terminal unit should be taken into account for the predominant factors that affect the redox reaction of the species in solution.[36] (a) By assuming that the modified monolayer phase corresponds to the compact layer in the Gouy–Chapman–Stern (GCS) model for an electrical double layer, the ionization of the terminal unit causes the shift of the diffuse layer potential, ϕ_2, at the electrode–electrolyte interface. Accordingly, the effective potential difference, $\phi_M - \phi_2$, driving the redox reaction is also shifted by the ionization of the terminal unit as depicted in Fig. 4. The positively charged terminal unit will cause the $\phi_M - \phi_2$ value to be more negative as compared with the neutral terminal unit. Therefore, the positive shift of the ϕ_2-potential brings about the decrease of the apparent reaction rate for the oxidation process. In contrast, the negatively charged terminal unit brings about the negative shift of the ϕ_2-potential and the increase of the apparent oxidation rate. The opposite effect of the charged unit is expected in the case of the reduction process. (b) The charged terminal unit also affects the distribution of the ionic redox species in the vicinity of the electrode surface, due to the electrostatic interaction between the terminal unit and redox species. The positively charged terminal unit will repels the cationic species from the electrode surface, while the negatively charged terminal will attract the cationic species. The opposite effect will be expected for the anionic redox species. Hereafter, we denote the effect of the ϕ_2-potential on the reaction rate as the ϕ_2-effect and the effect of the electrostatic interaction on the surface concentration as the electrostatic effect.

While the ϕ_2-effect changes the apparent heterogeneous rate constant of the charge transfer, the electrostatic effect changes the surface concentration of the ionized redox species. It should be noted that the ϕ_2-effect is affected only by the charge of the electrode surface but not by the charge of the redox species. In contrast, the electrostatic effect is decisively affected by the correlation between the surface charge and the charge of the electrode species.

The dependencies of the voltammetric responses on the modified monolayer shown in Figs. 1, 2, and 3 can be understood by considering the factors affecting the electrode process as described above and the charge of redox species. In the case of FcDM, no electrostatic effect would be expected because FcDM has no net charge. Therefore, the difference of the voltammetric responses in Fig. 1 is solely caused by the shift of the ϕ_2-potential. In the oxidation process of FcDM at AUT/Au, the positively charged terminal unit of AUT/Au will shift the ϕ_2-potential to be more positive as compared with the ϕ_2-potential of neutral MUO/Au. This shift of the ϕ_2-potential decreases the effective potential difference, $\phi_M - \phi_2$, driving the oxidation reaction. Accordingly, the observed reaction current will be lower at a AUT/Au than at a MUO/Au. The opposite effect of the terminal charge will be expected for the reaction at MUA/Au. The contribution of the ϕ_2-effect similar to FcDM reaction is expected even in the oxidation processes of FcMA and FcSA. However, the electrostatic interaction between redox species and terminal unit has the opposite effect for the responses of FcMA and FcSA. In the reaction of FcMA at AUT/Au, the electrostatic repulsion decreases the surface concentration of FcMA and decreases the voltammetric response. In contrast, the surface concentration of FcMA is increased by the electrostatic attraction when mea-

sured with MUA/Au and therefore the voltammetric response is also increased, as compared with the response at MUO/Au. The opposite electrostatic effect of the terminal charge is expected for the reaction of FcSA.

To compare quantitatively the correlation between the terminal charge and voltammetric response, the effect of a diffusion on the voltammetric response was corrected by using convolution techniques.[23,36,37] During the voltammetric experiments, the surface concentration of the initially present redox species (the reduced form of the ferrocene derivatives, in this case), C_r $(0,t)$, at time, t, can be expressed as

$$C_r(0,t) = C_r^* - (nFAC_r^* D_r^{1/2})^{-1} \int_0^t \frac{i(u)}{(t-u)^{1/2}} du, \quad (1)$$

where, C_r^* and D_r are the bulk concentration and diffusion coefficient of the initially present redox species, respectively, n is the number of electrons transferred in the electron transfer, A is the electrode area, and $i(u)$ is the electrode current at time u. Finally, the effect of diffusion limitation can be eliminated from the current–potential curve by multiplying the measured current by C_r^*/C_r $(0,\ t)$. The evaluation of Eq. 1 was made by a numerical integration technique using the algorithm reported by Lawson et al.[38] In the correction for diffusion limitation, the CV data were limited to the anodic wave and to the corrected current not in excess of a factor of 4 times larger than the uncorrected current. Figures 5, 6, and 7 show the current-potential curves of 2 mM FcDM, FcMA, and FcSA, respectively, corrected for diffusion limitation.

Effect of the Terminal Charge on the ϕ_2-Potential. The apparent heterogeneous rate constant, k_{app}, can be written as a function of the electrode potential as

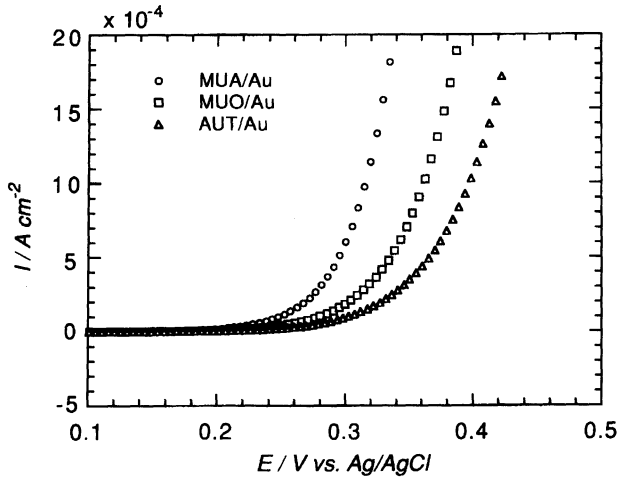

Fig. 5. Potential dependence of the diffusion corrected current, I_{cor}, for the anodic process of 2 mM FcDM in 0.2 M KCl aqueous solution. The I_{cor} values were calculated from the voltammetric data observed at MUA/Au, MUO/Au, and AUT/Au shown in Fig. 1.

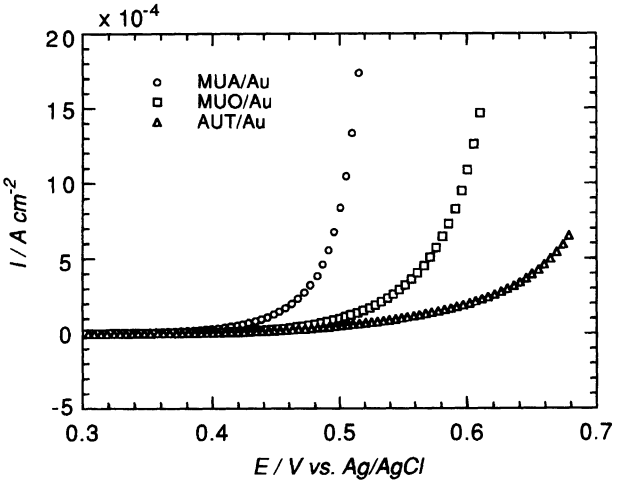

Fig. 6. Potential dependence of the diffusion corrected current, I_{cor}, for the anodic process of 2 mM FcMA in 0.2 M KCl aqueous solution. The I_{cor} values were calculated from the voltammetric data observed at MUA/Au, MUO/Au, and AUT/Au shown in Fig. 2.

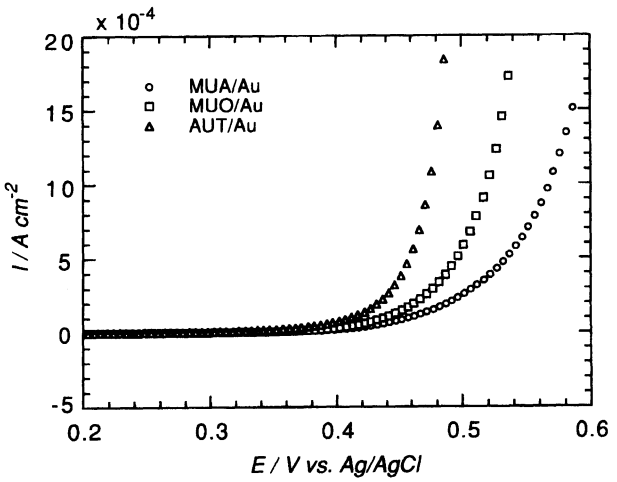

Fig. 7. Potential dependence of the diffusion corrected current, I_{cor}, for the anodic process of 2 mM FcSA in 0.2 M KCl aqueous solution. The I_{cor} values were calculated from the voltammetric data observed at MUA/Au, MUO/Au, and AUT/Au shown in Fig. 3.

$$k_{app} = k^0 \exp\left[\frac{\beta nF}{RT}(\eta - \phi_2)\right], \quad (2)$$

where k^0 is the standard heterogeneous rate constant, β is the transfer coefficient for the anodic process, and η is the overpotential. Further, the diffusion corrected current, I_{cor}, can be related with k_{app} as

$$I_{cor} = k_{app} nFC_s, \quad (3)$$

where C_s is the surface concentration of redox species. In the case of no electrostatic effect, the surface concentration, C_s, can be replaced with the bulk concentration of the redox species, C_b.

In the reaction of FcDM, as described in the previous section, the electrostatic effect can be neglected

and only the ϕ_2-effect should be taken into account to elucidate the potential dependence of the current response. To estimate the absolute value of the ϕ_2-potential, the potential of zero charge (pzc) should be obtained for each modified electrode. In this system, however, we could not be obtained a clear pzc value in spite of the effort to obtain with the following three different methods: (1) the voltammetric charging current measurements; (2) the heterogeneous rate constant measurements as a function of the supporting electrolyte concentration;[24] and (3) the impedance measurement. Alternatively, the relative change of the ϕ_2-potential caused by the charged terminal group can be estimated by comparing the current–potential responses between the different electrodes. In the reaction of FcDM at MUO/Au, the reaction current is unaffected by the terminal charge because the MUO terminal has no net charge. Therefore, the difference of the current–potential curves in Fig. 5 can be accounted for the shift of ϕ_2-potential caused by the terminal charges of MUA and AUT. From Eqs. 2 and 3, the relation between I_{cor} and ϕ_2 for each electrode can be written as

$$I_{cor}^{MUO} = nFC_b k_0 \exp\left[\frac{\beta nF}{RT}(\eta - \phi_2^{MUO})\right], \quad (4)$$

$$I_{cor}^{MUA} = nFC_b k_0 \exp\left[\frac{\beta nF}{RT}(\eta - \phi_2^{MUA})\right], \quad (5)$$

$$I_{cor}^{AUT} = nFC_b k_0 \exp\left[\frac{\beta nF}{RT}(\eta - \phi_2^{AUT})\right], \quad (6)$$

where the superscripts MUO, MUA, and AUT indicate the values of I_{cor} and ϕ_2 obtained at MUO/Au, MUA/Au, and AUT/Au electrodes, respectively. With the assumption that the β value is scarcely affected by the terminal group of the monolayer, the difference of the ϕ_2 value between the MUA/Au and MUO/Au is obtained from Eqs. 4 and 5 as

$$\Delta\phi_2^{MUA} = -\frac{RT}{\beta nF}\ln(I_{cor}^{MUA}/I_{cor}^{MUO}) \quad (7)$$

and the difference between AUT/Au and MUO/Au is obtained from Eqs. 4 and 6 as

$$\Delta\phi_2^{AUT} = -\frac{RT}{\beta nF}\ln(I_{cor}^{AUT}/I_{cor}^{MUO}), \quad (8)$$

where $\Delta\phi_2^{MUA} = \phi_2^{MUA} - \phi_2^{MUO}$ and $\Delta\phi_2^{AUT} = \phi_2^{AUT} - \phi_2^{MUO}$.

Figure 8 shows the potential dependence of $\Delta\phi_2^{MUA}$ and $\Delta\phi_2^{AUT}$ calculated from the Eqs. 7 and 8, respectively, by using the I_{cor} values in Fig. 5. In calculation, the β values of the FcDM oxidation were obtained from the Tafel plots of the I_{cor} to be 0.78±0.1 for all the modified electrodes examined. Figure 9 shows the potential dependence of the simulated current, $I_{sim,1}$, of FcDM, in which the $I_{sim,1}$ values at a MUA/Au and an AUT/Au were calculated from the observed I_{cor} value at a MUO/Au by using Eqs. 7 and 8, respectively, and the $\Delta\phi_2$ values in Fig. 8. In the calculation of $I_{sim,1}$, $\Delta\phi_2^{MUA}$ and $\Delta\phi_2^{AUT}$ values were approximated by the

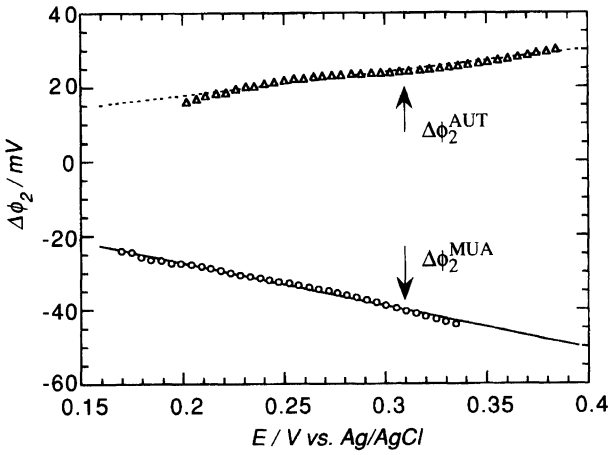

Fig. 8. Potential dependence of the difference of the diffuse layer potential, $\Delta\phi_2$, between MUO/Au and MUA/Au ($\Delta\phi_2^{MUA} = \phi_2^{MUA} - \phi_2^{MUO}$), and between MUO/Au and AUT/Au ($\Delta\phi_2^{AUT} = \phi_2^{AUT} - \phi_2^{MUO}$) calculated from the I_{cor} values for the oxidation of FcDM. The lines in figure are the results of linear regression which were used to the simulation of current–potential curves.

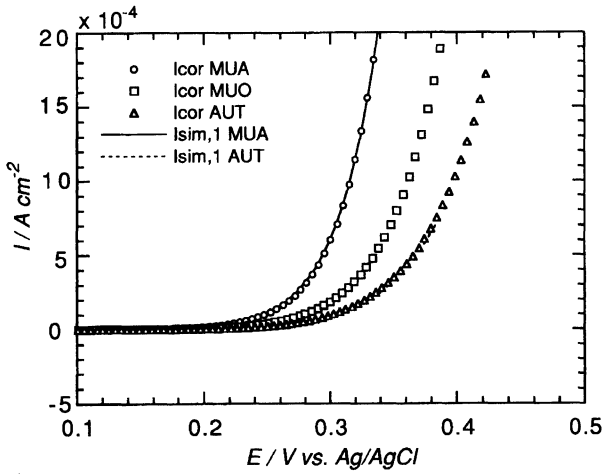

Fig. 9. Potential dependence of the simulated current for the reaction of FcDM at the MUA/Au and at the AUT/Au. The currents $I_{sim,1}^{MUA}$ and $I_{sim,1}^{AUT}$ were simulated from the I_{cor} value observed at the MUO/Au by taking the ϕ_2-effect into account.

linear regression lines as depicted in Fig. 8. However, the coincidence between observed currents and simulated currents indicates the validity of the linear approximation of the $\Delta\phi_2^{MUA}$ and $\Delta\phi_2^{AUT}$ values.

By assuming fully ionized terminal units and a densely packed monolayer, the $\Delta\phi_2^{MUA}$ and $\Delta\phi_2^{AUT}$ values are estimated to be −175 and 175 mV, respectively, on the bases of Gouy–Chapman theory.[36,39] On the other hand, the observed $\Delta\phi_2$ values are far smaller than the above estimation, as shown in Fig. 8. This result indicates that the large portion of the terminal charge is compensated with the ionic species in solution for both MUA/Au and AUT/Au.

Effects of $\Delta\phi_2$-Potential on the Surface Concentration, C_s, of FcSA and FcMA. In the reaction of FcSA and FcMA, the effect of the electrostatic interaction between the electrode surface and redox species on the surface concentration of these species should be taken into account, because FcSA and FcMA have negative and positive net charges, respectively. The surface concentration of the ionized electroactive species, C_s, can be related to the bulk concentration, C_b, by using the ϕ_2-potential as

$$C_s = C_b \exp(-zF\phi_2/RT) \quad (9)$$

where z is the charge of the electroactive species ($z=1$ for FcMA and $z=-1$ for FcSA). In contrast to that, the ϕ_2-effect does not depend on the charge of electroactive species (cf. Eqs. 4 to 6), the electrostatic effect highly depends on the charge of electroactive species. By taking the electrostatic effect into account, to Eqs. 4 to 6 can be rewritten as

$$I_{cor}^{MUO} = nFC_b k_0 \exp\left[\frac{\beta nF}{RT}\eta - \frac{(\beta n+z)F}{RT}\phi_2^{MUO}\right], \quad (10)$$

$$I_{cor}^{MUA} = nFC_b k_0 \exp\left[\frac{\beta nF}{RT}\eta - \frac{(\beta n+z)F}{RT}\phi_2^{MUA}\right], \quad (11)$$

$$I_{cor}^{AUT} = nFC_b k_0 \exp\left[\frac{\beta nF}{RT}\eta - \frac{(\beta n+z)F}{RT}\phi_2^{AUT}\right]. \quad (12)$$

With the assumption that the β value is not changed by the terminal unit, the I_{cor}^{MUA} can be expressed using the I_{cor}^{MUO} values by dividing Eq. 11 by Eq. 10 as

$$I_{cor}^{MUA} = I_{cor}^{MUO} \exp\left[-\frac{(\beta n+z)F}{RT}\Delta\phi_2^{MUA}\right] \quad (13)$$

and similarly the I_{cor}^{AUT} is expressed as

$$I_{cor}^{AUT} = I_{cor}^{MUO} \exp\left[-\frac{(\beta n+z)F}{RT}\Delta\phi_2^{AUT}\right]. \quad (14)$$

From Eqs. 13 and 14 and using the observed $\Delta\phi_2$ values shown in Fig. 8, the potential dependence of the I_{cor}^{MUA} and I_{cor}^{AUT} can be simulated from the observed potential dependence of the I_{cor}^{HUM} value (denote the simulated current using Eqs. 13 or 14 as the $I_{sim,2}$). The β values of FcSA and FcMA obtained from Tafel plots are 0.63±0.05 and 0.67±0.07, respectively, for all the modified electrodes examined.

Figures 10 and 11 show the potential dependencies of $I_{sim,2}^{MUA}$ and $I_{sim,2}^{AUT}$, respectively, for the reaction of FcSA. The figures also show the potential dependencies of $I_{sim,1}^{MUA}$ and $I_{sim,1}^{AUT}$, respectively, in which the currents were simulated using Eqs. 7 or 8. In the case of $I_{sim,1}^{MUA}$ and $I_{sim,1}^{AUT}$, therefore, only the ϕ_2-effect is taken into account and the electrostatic effect is neglected. As shown in theses figures, the correction of ϕ_2-effect brings about the increase of the difference between the simulated current ($I_{sim,1}$) and the observed current (I_{cor}) for the both of MUA/Au and AUT/Au. Contrary to it, the correction of electrostatic effect greatly reduces the difference between the simulated current ($I_{sim,2}$) and the observed

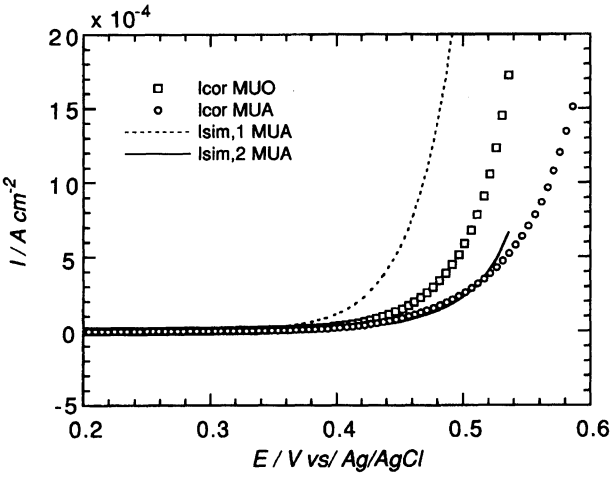

Fig. 10. Potential dependence of the simulated current for the reaction of FcSA at the MUA/Au. The $I_{sim,1}^{MUA}$ and $I_{sim,2}^{MUA}$ values were simulated from the I_{cor} value observed at the MUO/Au. In the calculation of $I_{sim,1}^{MUA}$, only the ϕ_2-effect was taken into account. In the calculation of $I_{sim,2}^{MUA}$, both the ϕ_2-effect and the electrostatic effect were taken into account.

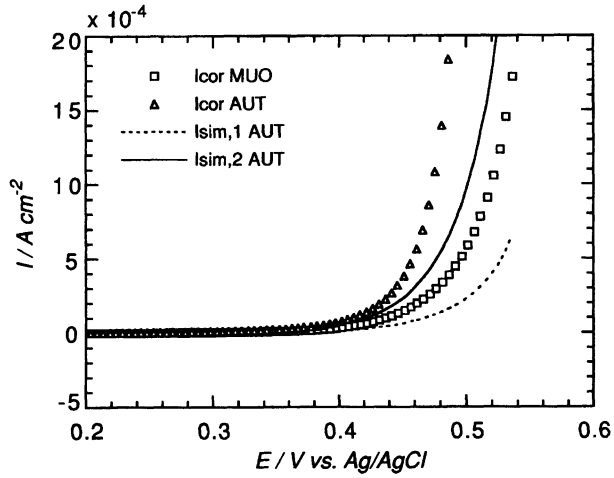

Fig. 11. Potential dependence of the simulated current for the reaction of FcSA at the AUM/Au. The $I_{sim,1}^{AUT}$ and $I_{sim,2}^{AUT}$ values were simulated from the I_{cor} value observed at the MUO/Au. In the calculation of $I_{sim,1}^{AUT}$, only the ϕ_2-effect was taken into account. In the calculation of $I_{sim,2}^{AUT}$, both the ϕ_2-effect and the electrostatic effect were taken into account.

current (I_{cor}). These results can be explained by considering the correlation between the terminal charge and the ionic state of the electroactive species. In the reaction of FcSA at MUA/Au (Fig. 10), the negatively charged MUA surface causes the shift of ϕ_2-potential to a more negative value and the shift of $\phi_M - \phi_2$ value to be more positive, as compared with the neutral MUO surface. Therefore, the correction of the ϕ_2-effect to the current observed at neutral MUO/Au (I_{cor}^{MUO}) resulted in the increase of the simulated current ($I_{sim,1}^{MUA}$). Contrary to this, the electrostatic repulsion between the

negatively charged FcSA and MUA surface decreases the surface concentration of FcSA and accordingly the decrease of the simulated current ($I_{sim,2}^{MUA}$).

In the reaction of FcSA at AUT/Au, in contrast to the case of MUA/Au, the positively charged AUT surface decreases the $\phi_M - \phi_2$ value and accordingly decreases the $I_{sim,1}^{AUT}$. In contrast, the electrostatic interaction increases the surface concentration of the negatively charged FcSA and also increases the $I_{sim,2}^{AUT}$ value (Fig. 11).

Figures 12 and 13 show the simulation results for the reaction of FcMA. In the reaction of FcMA at MUA/Au, both the ϕ_2-effect and electrostatic effect increase the simulated current ($I_{sim,1}^{MUA}$ and $I_{sim,2}^{MUA}$, respectively), as compared with the reaction current at neutral MUO/Au (I_{cor}^{MUO}), because the negatively charged MUA surface increases both of the $\phi_M - \phi_2$ value and the surface concentration of positively charged FcMA. In the reaction at AUT/Au, in contrast, the positively charged AUT surface decreases the $\phi_M - \phi_2$ value. Furthermore, the electrostatic repulsion between AUT surface and FcMA also decreases the surface concentration of FcMA. Both of these factors decrease the simulated current ($I_{sim,1}^{AUT}$ and $I_{sim,2}^{AUT}$, respectively) as compared with the reaction current at MUO/Au (I_{cor}^{MUO}). These effects are reflected in the simulation curves shown in Figs. 12 and 13. However, the I_{cor} curve lies between the $I_{sim,1}$ and $I_{sim,2}$ curves for both reactions at MUA/Au and AUT/Au. These results indicate that the correction for electrostatic effect overestimated the electrostatic interaction. Although we have no clear explanation for this, the molecular structure of the FcMA is a possibility. The redox active ferrocenyl unit of the FcMA is separated from the charged trimethylammonium unit by a methylene unit and moreover the positively charged nitrogen atom is surrounded by neutral methyl units. This structure of FcMA reduces the effect of the electrostatic interaction between the monolayer terminal unit and the FcMA trimethyl unit on the electrode process of ferrocenyl unit, in contrast to that, the ϕ_2-effect is not affected by the charge of the FcMA. On the other hand, the $I_{sim,2}$ values of FcMA were calculated by assuming a positive unit charge of FcMA, which may have resulted in the overestimation of the electrostatic effect. To measure the effects of electrostatic interaction more precisely, the effective charge of the redox species contributing the interaction should be introduced in the simulation.

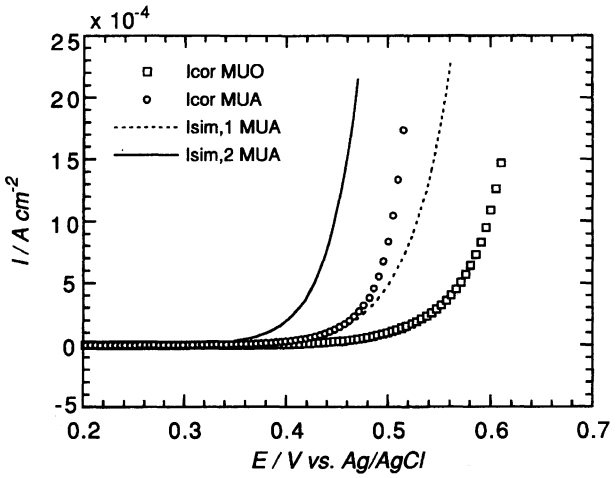

Fig. 12. Potential dependence of the simulated current for the reaction of FcMA at the MUA/Au. The $I_{sim,1}^{MUA}$ and $I_{sim,2}^{MUA}$ values were simulated from the I_{cor} value observed at the MUO/Au. In the calculation of $I_{sim,1}^{MUA}$, only the ϕ_2-effect was taken into account. In the calculation of $I_{sim,2}^{MUA}$, both the ϕ_2-effect and the electrostatic effect were taken into account.

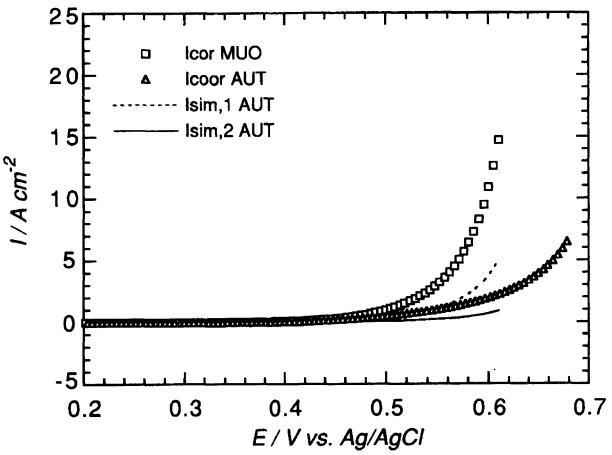

Fig. 13. Potential dependence of the simulated current for the reaction of FcMA at the AUT/Au. The $I_{sim,1}^{AUT}$ and $I_{sim,2}^{AUT}$ values were simulated from the I_{cor} value observed at the MUO/Au. In the calculation of $I_{sim,1}^{AUT}$, only the ϕ_2-effect was taken into account. In the calculation of $I_{sim,2}^{AUT}$, both the ϕ_2-effect and the electrostatic effect were taken into account.

It must be noted that the effect of the terminal unit on the monolayer packing density should also be taken into account for more detailed discussion. The charged terminal units of MUA and AUT will hinder the densely packing of the monolayers, as compared with the neutral MUO. This difference in the packing state also affects the redox behavior at the monolayer surface. Studies on the effects of the terminal unit on the packing state are now in progress in our laboratory, using a quartz crystal micro balance technique.

Conclusions

Electrochemical investigations of the terminally substituted alkanethiol monolayer assembly made clear the contribution of the ϕ_2-potential and the electrostatic interaction on the redox process. The effect of the terminal charge on the ϕ_2-potential was estimated from the reaction of neutral FcDM at differently charged X-alk/Au electrodes. The obtained $\Delta\phi_2$ values indicate that a large portion of the terminal charges is compensated by the ionic species in solution. By using the

obtained values of $\Delta\phi_2$, the effect of electrostatic interaction was estimated and also simulated the current-potential curves, taking the ϕ_2-effect and the electrostatic effect into account. In the reaction of FcSA at MUA/Au and at AUT/Au, the simulation well reproduced the observed current–potential behavior. In the case of FcMA, however, the simulation resulted in the overestimation of the electrostatic effect. This overestimation is accounted for the reduced effective charge of the FcMA molecule caused by its structure. We demonstrated in this paper the validity of the monolayer modified electrode for the study of the electrode-electrolyte interface.

This work is funded in part by the CASIO Science Promotion Foundation (K.T.) to whom we are grateful.

References

1) M. D. Porter, T. B. Bright, D. L. Allara, and C. E. D. Chidsey, *J. Am. Chem. Soc.*, **109**, 3559 (1987).
2) C. D. Bain, J. Evall, and G. M. Whitesides, *J. Am. Chem. Soc.*, **111**, 7155 (1989).
3) C. D. Bain and G. M. Whitesides, *J. Am. Chem. Soc.*, **111**, 7164 (1989).
4) L. H. Dubois, B. R. Zegarski, and R. G. Nuzzo, *J. Am. Chem. Soc.*, **112**, 570 (1990).
5) S. D. Evans and A. Ulman, *Chem. Phys. Lett.*, **170**, 462 (1990).
6) S. D. Evans, B. K. E. Goppert, E. Urankar, L. J. Gerenser, A. Ulman, and R. G. Snyder, *Langmuir*, **7**, 2700 (1991).
7) C. E. D. Chidsey and D. N. Loiacono, *Langmuir*, **6**, 682 (1990).
8) C. A. Widrig, C. A. Alves, and M. D. Porter, *J. Am. Chem. Soc.*, **113**, 2805 (1991).
9) K. L. Prime and G. M. Whitesides, *Science (Washington, D. C.)*, **252**, 1164 (1991).
10) S. D. Evans, E. Urankar, A. Ulman, and N. Ferris, *J. Am. Chem. Soc.*, **113**, 4121 (1991).
11) L. J. Kepley, *Anal. Chem.*, **64**, 3191 (1992).
12) J. Wang, L. M. Frostman, and M. D. Ward, *J. Phys. Chem.*, **96**, 5224 (1992).
13) J. Xu, H. Li, and Y. Zhang, *J. Phys. Chem.*, **97**, 11497 (1993).
14) G. Y. Liu and M. B. Salmeron, *Langmuir*, **10**, 367 (1994).
15) J. J. Hichman, D. Ofer, C. Zou, and M. S. Wrighton, *J. Am. Chem. Soc.*, **113**, 1128 (1991).
16) E. W. Wollman, D. Kang, C. D. Frisbie, I. M. Ivan, and M. S. Wrighton, *J. Am. Chem. Soc.*, **116**, 4395 (1994).
17) L. F. Rozsnyai and M. S. Wrifhton, *J. Am. Chem. Soc.*, **116**, 5993 (1994).
18) C. E. D. Chidsey, C. R. Bertozzi, T. M. Putvinski, and A. M. Mujsce, *J. Am. Chem. Soc.*, **112**, 4301 (1990).
19) K. A. Bunding Lee, *Langmuir*, **6**, 709 (1990).
20) H. O. Finklea and D. D. Hanshew, *J. Am. Chem. Soc.*, **114**, 3173 (1992).
21) E. Katz, N. Itzhak, and I. Willner, *Langmuir*, **9**, 1392 (1993).
22) C. Miller, P. Cuendet, and M. Graetzel, *J. Phys. Chem.*, **95**, 877 (1991).
23) A. M. Becka and C. J. Miller, *J. Phys. Chem.*, **96**, 2657 (1992).
24) A. M. Becka and C. J. Miller, *J. Phys. Chem.*, **97**, 6233 (1993).
25) R. Bilewicz and M. Majda, *J. Am. Chem. Soc.*, **113**, 5464 (1991).
26) R. Bilewicz and M. Majda, *Langmuir*, **7**, 2794 (1991).
27) K. Takehara, Y. Ide, and M. Aihara, *Bioelectrochem. Bioenerg.*, **29**, 113 (1992).
28) K. Takehara, Y. Ide, E. Obuchi, and M. Aihara, *Bioelectrochem. Bioenerg.*, **29**, 103 (1992).
29) F. Malem and D. Mandler, *Anal. Chem.*, **65**, 37 (1993).
30) I. Turyan and D. Mandler, *Anal. Chem.*, **66**, 58 (1994).
31) O. Chailapakul and R. M. Crooks, *Langmuir*, **9**, 884 (1993).
32) K. Takehara, H. Takemura, and Y. Ide, *Electrochim. Acta*, **39**, 817 (1994).
33) M. Cefola, A. S. Tompa, A. V. Celiano, and P. S. Gentile, *Inorg. Chem.*, **1**, 290 (1962).
34) Y. Tuchitani, T. Ando, and K. Ueno, *Bull. Chem. Soc. Jpn.*, **36**, 1534 (1963).
35) M. Niwa, M. Shimoguchi, and N. Higashi, *J. Colloid Interface Sci.*, **148**, 592 (1992).
36) A. J. Bard and L. R. Faulkner, "Electrochemical Methods; Fundamentals and Applications," Wiley, New York (1980), p. 540.
37) J. C. Imbeaux and J. M. Saveant, *J. Electroanal. Chem.*, **44**, 1969 (1973).
38) R. J. Lawson and J. T. Maloy, *Anal. Chem.*, **46**, 559 (1974).
39) L. Strong and G. M. Whitesides, *Langmuir*, **4**, 546 (1988).